DAVE

Data Analysis and Visualization Environment

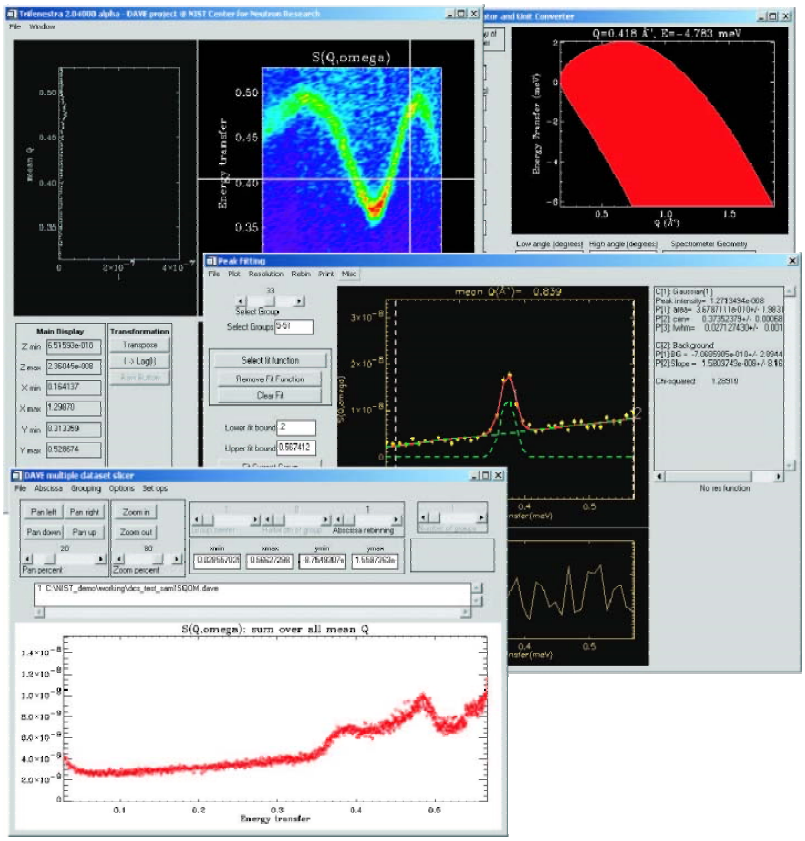

DAVE is an integrated environment for the reduction, visualization and analysis of inelastic neutron scattering data. It is built using IDL (Interactive Data Language) from Research Systems, Inc. which is a cross-platform application development tool with built-in graphics. All efforts have been made to ensure that DAVE is supported on Linux, Windows and MacOS9. It is available at no cost to users in two forms. The first is as a binary executable with an embedded IDL runtime license which can be used by anyone running on any of the three supported operating systems. In addition, for those who have an IDL development license, the complete source code for DAVE is also available. The main objective of DAVE is to provide a user friendly tool for scientists involved in neutron scattering research to quickly reduce, visualize and intepret their data. Currently, much progress has been made towards achieving this goal even though a lot still remains to be done. Support for several neutron scattering spectrometers at NCNR have been included.

The following are some of the features that are presently available in DAVE:

Reduction
Data reduction modules are available for the following NCNR instruments:

- Triple axis spectrometers: SPINS
- Filter analyser spectrometer: FANS
- TOF chopper spectrometer: DCS
- Backscattering spectrometer: HFBS

Visualization
Modules are available which provide:

- Color image (2 dimensional) displays of data
- Ability to rebin and also make 1D slices/cuts of 2D data along the x- or y-axis
- Generate hardcopy (color) output in postscript and jpeg formats

Analysis
A comprehensive menu-driven curve fitting module is available which:

- takes into account the instrumental resolution function
- has a large selection of useful model functions
- automates multi-detector fitting of 2D data
- generates hardcopy of the fits
- saves fit parameters in an ASCII file

Other
Other modules are available, such as:

- Spurion calculator for determining the location of spurious inelastic peaks for Triple Axis spectrometers
- Eigenvalue and hindered rotational dynamics calculator for molecular rotors (hydrogen, methyl systems)
- Self-shielding corrections calculator
- Digitizer for extracting data points from a plot or image

Pressure-Induced Phase Transition of $C_{12}E_5$ Micelles

Nonionic surfactants form a variety of microstructures in water, ranging from simple micelles at low surfactant concentrations to complex mesophases, such as hexagonal or lamellar phases at high concentrations. The effect of pressure on the structure of micelles and microemulsions has not been extensively studied. Small angle neutron scattering (SANS) is particularly well suited for such measurements because the range of length scales probed includes both the particle size and the interparticle spacing.

Pressure effects observed in SANS measurements of surfactant microstructure are typically interpreted in terms of geometric packing arguments that focus on the compressible hydrophobic tails of the surfactants. In this context, increasing pressure has the single effect of decreasing the surfactant tail volume, thereby increasing the curvature of the oil-water interface. Conversely, increasing temperature dehydrates the nonionic headgroups, decreasing the headgroup area and decreasing the film curvature. Thus, temperature and pressure can be viewed as thermodynamic variables with inherently different mechanisms and opposite effects for controlling microstructure in nonionic surfactant solutions.

Here we report the results of high-pressure SANS experiments at 20 °C and pressures up to ≈ 300 MPa on a solution of pentaethylene glycol mono-n-dodecyl ether ($C_{12}E_5$) in D_2O having a mass fraction of 1 %. The phase diagram for this system [1] at ambient pressure is shown in Fig. 1. At this temperature and surfactant concentration, a single-phase micellar solution (L_1 phase) forms at ambient pressure, well below the lower critical solution temperature (LCST) for liquid-liquid equilibrium and far removed from the H_1 hexagonal phase at much higher $C_{12}E_5$ concentrations. The microstructure of the L_1-phase at ambient pressure is known to be a network of branched semi-flexible, cylindrical micelles with the branch points comprised of three-armed junctions.

SANS spectra were measured using the NIST high-pressure cell and neutrons of wavelength $\lambda = 6$ Å, covering a q-range of $0.012\ \text{Å}^{-1} < q < 0.22\ \text{Å}^{-1}$. The scattering curves obtained at 3.4 MPa, 241 MPa, and 255 MPa are shown in Fig. 2. The curves at 3.4 Mpa and 241 MPa are virtually identical, indicating no significant change in microstructure with increasing pressure up to 241 MPa. Fitting these curves using a form factor for cylindrical micelles gives a radius of (21.0 ± 0.2) Å and a length greater than 600 Å, independent of pressure. However, a small increase in pressure from 241 MPa to 255 MPa leads to the appearance of a peak in the scattering intensity at $q \approx 0.130\ \text{Å}^{-1}$, indicative of a locally ordered system. A similar transition has been reported in high-pressure SANS studies of tetradecyldimethylaminoxide (TDMAO) micelles in D_2O at pressures up to 300 MPa, but the high-pressure microstructure was never determined [2].

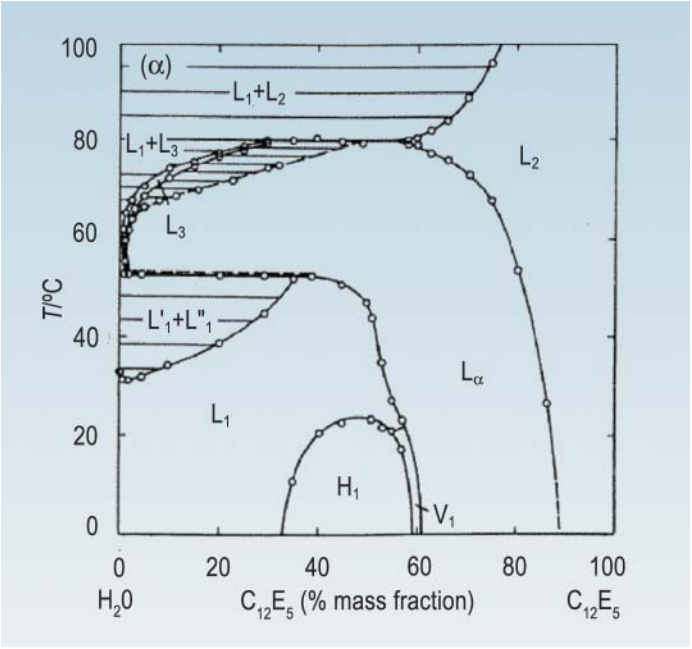

FIGURE 1. Temperature-composition phase diagram for $C_{12}E_5$/water solutions at ambient pressures [1].

Shown in Fig. 2 is the scattering curve for the H_1 hexagonal phase at 49 % $C_{12}E_5$ mass fraction at 20 °C, and ambient pressure. The peak at $q \approx 0.120\ \text{Å}^{-1}$, arising from the hexagonal lattice of cylindrical micelles, is similar to the peak for the 1 % $C_{12}E_5$ mass fraction solution at 255 MPa, suggesting that this new high-pressure phase may resemble a slightly compressed state of the H_1 hexagonal phase at ambient pressure. The formation of a lamellar phase from cylindrical micelles is unlikely, since this corresponds to increasing the hydrophobic core volume-to-surface-area ratio per surfactant molecule, or equivalently, decreasing the spontaneous curvature of the surfactant film. The application

D. P. Bossev and M. E. Paulaitis
Department of Chemical Engineering
Johns Hopkins University
Baltimore, Maryland 21228-2694

J. N. Israelachvili
Department of Chemical Engineering
University of California, Santa Barbara
Santa Barbara, CA 93106

S. R. Kline
NIST Center for Neutron Research
National Institute of Standards and Technology
Gaithersburg, MD 20899-8562

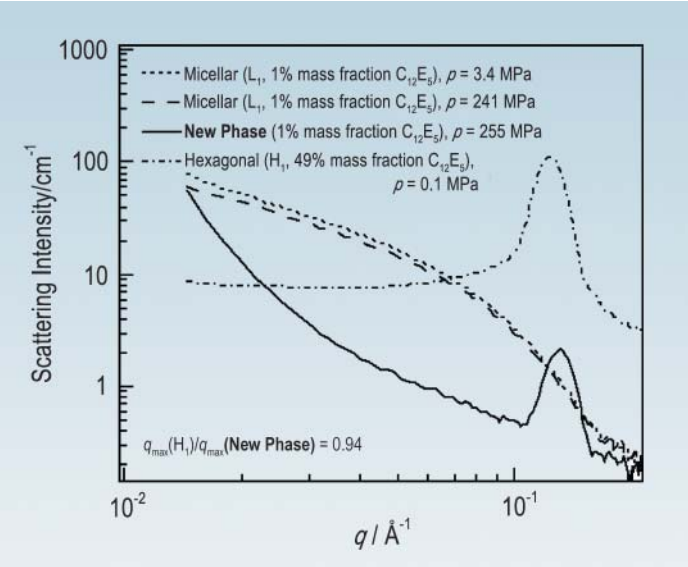

FIGURE 2. Measured SANS spectra at 20 °C for 1 % mass fraction $C_{12}E_5$ in D_2O as a function of pressure and 49 % mass fraction $C_{12}E_5$ in D_2O at ambient pressure.

of pressure would have the opposite effect. We conclude, therefore, that the observed change in microstructure corresponds to a pressure-induced L_1-H_1 phase transition from a network of branched semi-flexible, cylindrical micelles to hexagonally ordered bundles of cylindrical micelles.

To further understand the SANS results, we have measured the temperature dependence of the L_1-H_1 transition pressure and find that the *p*-*T* curve follows the *p*-*T* freezing curves for liquid *n*-alkanes of comparable hydrocarbon chain length. *N*-decane solidifies at a pressure of $\approx$ 250 MPa at 20 °C, which is close to the pressure for the observed L_1-H_1 phase transition. We propose that the $C_{12}E_5$ micelle hydrophobic core, equivalent to *n*-decane, does solidify at these conditions, such that the micelles lose flexibility, and hence conformational entropy. An analysis of the geometric packing constraints for three-arm junctions coexisting with cylinders shows that when the surfactant tail volume decreases with increasing pressure, the fraction of surfactant forming junction points also decreases. This indicates that the formation of three-arm junctions becomes increasingly unfavorable at higher pressures due to the compression of the $C_{12}E_5$ micelle hydrophobic core. Our calculations predict that no junctions should be present at $P > 275$ MPa at 20 °C, which is in good agreement with our observation of a structural transition between 241 MPa and 255 MPa at this temperature. Consequently, the network of branched thread-like micelles becomes globally unstable. The formation of hexagonally ordered bundles of cylindrical micelles follows as the attractive van der Waals forces between the micelles are not offset by entropic repulsive undulation interactions that are not present in the now-solidified hydrophobic core.

The practical significance of these results is to show that pressure allows access to regions of the $C_{12}E_5$/water phase diagram that are virtually inaccessible to temperature. Thus, the use of pressure may offer unique approaches for directing and stabilizing certain surfactant microstructures that, in turn, could prove useful for creating novel soft materials.

References

[1] R. Strey, R. Schomäcker, D. Roux, F. Nallet, U. Olsson, J. Chem. Soc. Faraday Trans. **86**, 2253 (1990).

[2] N. Gorski, J. Kalus, D. Schwahn, Langmuir **15**, 8080 (1999).

Atomic Motions in Confined Polymer Films

Material properties at surfaces and interfaces often deviate from their bulk values. An example is viscoelastic properties that are important in many applications such as chemically amplified photoresists, lubricants, adhesives, etc. A viscosity increase of a liquid polymeric film, like those used for hard disc lubricants, could have deleterious consequences. Likewise, a viscosity decrease in a thin photoresist film could enhance photoacid diffusion and create image blur. It is clearly important to characterize the molecular level mobility in thin polymer films. Of particular interest are changes in the glass transition temperature T_g, since the glass transition corresponds to a sharp change in viscosity.

It is well known that atomic thermal motions lead to a decrease in the intensity of the elastically scattered neutrons. In a harmonic solid the intensity is related to the amplitude of the motion through the Debye-Waller factor, $I_{inc}(Q) \sim exp(-\frac{1}{3}Q^2\langle u^2\rangle)$, where Q is the scattering vector and $\langle u^2\rangle$ is the mean-square atomic displacement. In a logarithmic plot of I_{inc} as a function of Q^2, $\langle u^2\rangle$ is proportional to the slope of a linear fit to the data. This approximation has proven very useful in studying the dynamics of polymers, both synthetic [1] and biological [2], despite the fact that their atomic motions are typically anharmonic.

The elastic incoherent neutron scattering intensities can be measured as a function of temperature on the NCNR's High Flux Backscattering Spectrometer (HFBS), using the "Fixed Window" mode. Polycarbonate (PC) films, seen in Fig. 1, are spin cast onto Si wafers, sectioned into small rectangles, and stacked into an Al sample cell. The scattering from the Si substrates and Al cell are negligible because their Bragg peaks are beyond the Q range of the instrument ($0.25\ Å^{-1} < Q < 1.75\ Å^{-1}$); the scattering is dominated by the large incoherent cross-section of the amorphous PC.

Ideally there should be 200 mg of PC per cell to maximize the signal and minimize multiple scattering effects (90 % transmission). For the Si-supported films we are limited by 0.5 mg to 10 mg of PC per cell and a thus obtain a very weak signal (99 % transmission). However, the HFBS is sufficiently sensitive to observe this signal, as seen in Fig. 2 where the temperature dependence of the elastic scattering is shown. The relative magnitude of the intensity

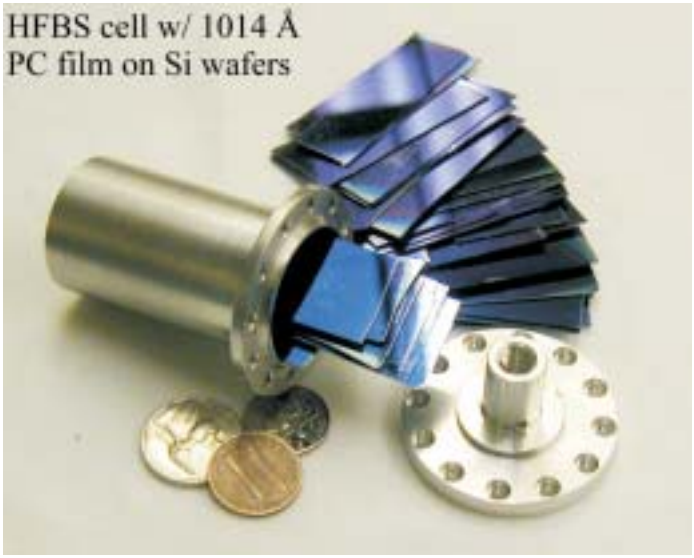

FIGURE 1. A stack of 1014 Å PC films (notice the blue tint) on thin slabs of Si ready to go into the HFBS spectrometer.

change diminishes with decreasing film thickness, a clear indication of reduced atomic mobility in the thin PC films. Given the HFBS energy resolution of 0.85 μeV, these intensity changes reflect changes in atomic motions at frequencies of 200 MHz or faster.

This reduced mobility is qualitatively reflected in Fig. 3 as strong suppression of $\langle u^2\rangle$. We emphasize qualitatively because $\langle u^2\rangle$ arises from a harmonic approximation. Nevertheless, there is a clear reduction in the amplitudes of the thermal motions, both above and below the calorimetric T_g, as the film thickness approaches the root-mean-square (rms) end-to-end length of PC (R_{ee} = 160 Å).

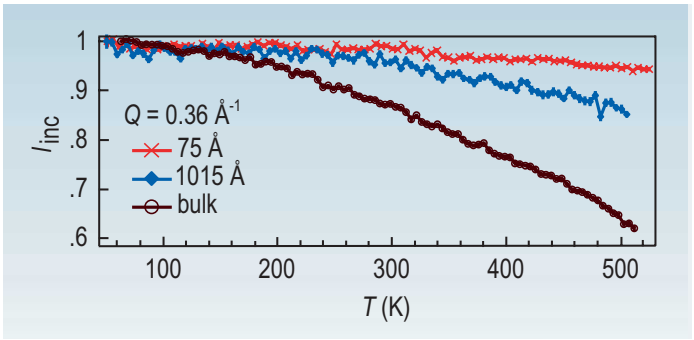

FIGURE 2. The normalized elastic intensities in the HFBS detector at Q = 0.36 Å^{-1}. The decrease in intensity at high temperatures reflects the presence of atomic motion in the thin polymer films.

C. L. Soles, J. F. Douglas, and Wen-li Wu
Polymers Division
National Institute of Standards and Technology
Gaithersburg, MD 20899-8541

R. M. Dimeo
NIST Center for Neutron Research
National Institute of Standards and Technology
Gaithersburg, MD 20899-8562

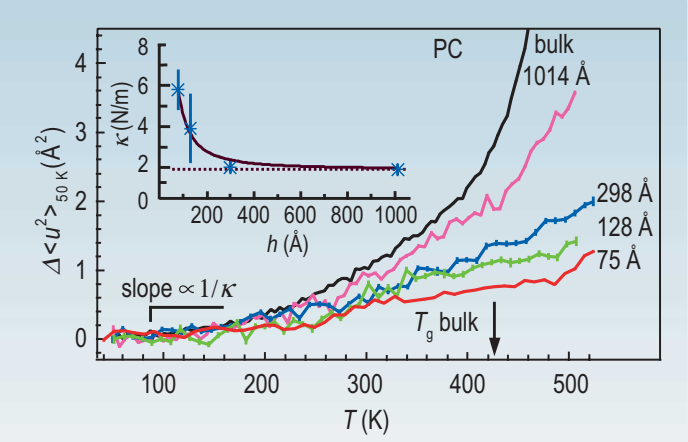

FIGURE 3. $\langle u^2\rangle$ as a function of temperature for the PC thin films. The inset reveals a stiffening of the harmonic (low temperature) force constant κ with decreasing film thickness h.

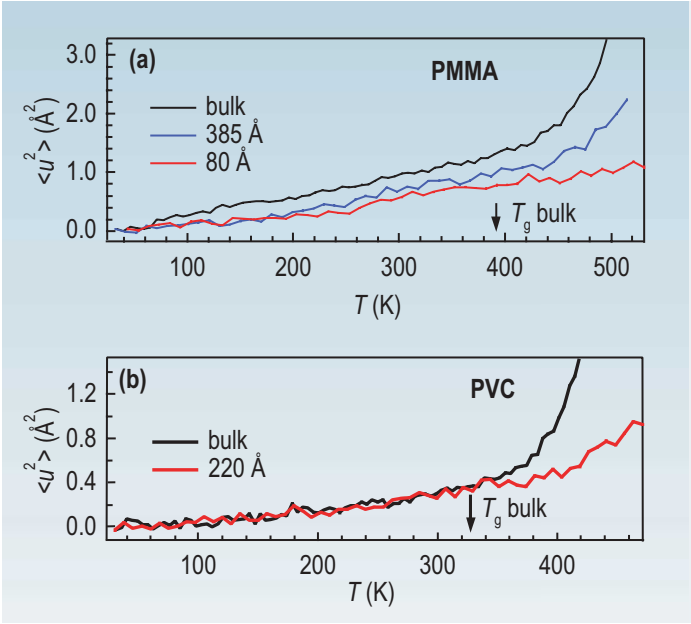

FIGURE 4. $\langle u^2\rangle$ as a function of thickness and temperature for similar PMMA (a) and PVC (b) films.

At temperatures below 200 K, $\langle u^2\rangle$ is small and the harmonic approximation is reasonable. In this regime the inverse of the slope of $\langle u^2\rangle$ vs. T is proportional to an elastic force constant κ. The inset of Fig. 3 displays a dramatic stiffening of κ with confinement. This implies that the atoms or molecules in PC become strongly caged by their environment in the thinner films.

Similar $\langle u^2\rangle$ measurements on thin films of polymethyl methacrylate (PMMA; R_{ee} = 915 Å) and polyvinyl chloride (PVC; R_{ee} = 437 Å) are shown in Figs. 4(a) and 4(b). There is a suppression of $\langle u^2\rangle$ with decreasing film thickness above the bulk T_g that is qualitatively consistent with the PC films. However, below the T_g for bulk PMMA the suppression is less pronounced, and not observed in the PVC films. Careful inspection of Figs. 3 and 4 suggests a relation between the magnitude of $\langle u^2\rangle$ at T_g in the bulk and the degree of $\langle u^2\rangle$ suppression in the thin glassy films.

Bulk PC has the largest $\langle u^2\rangle$ at T_g, indicating extensive mobility. In fact, PC is well known for its segmental mobility in the glassy state, which is in part related to its superior impact resistance. Molecular mobility helps dissipate strain energy. (PC is used in bullet-proof glass.) This extensive mobility is also susceptible to thin film confinement, as also seen through the stiffening of the elastic constants from 1.9 N/m in bulk PC to 5.8 N/m in the 75 Å film. At the other extreme, bulk PVC has the smallest $\langle u^2\rangle$ at T_g, indicating a lack of motions to be affected by confinement. This is also consistent with the strong intermolecular caging at low temperatures; both bulk PVC and the 220 Å film have large elastic force constants of 4.6 N/m. This lack of mobility reflects the observation that PVC is a brittle polymer that needs high levels of plasticization for practical use. Only when PVC is taken above the bulk T_g, where long-range motions dominate, do the effects of confinement become evident.

In short, we have seen two different responses to thin film confinement. While there is a general suppression of $\langle u^2\rangle$ and the fast dynamics, polymers with greater mobility are more susceptible to confinement, especially below the calorimetric T_g. In contrast, polymers with strongly localized motions appear bulk-like, even in highly confined glassy films. More details of these studies can be found in our upcoming publications [3–5].

References

[1] B. Frick, D. Richter, Science **267**, 1939 (1995).

[2] G. Zaccai, Science **288**, 1604 (2000).

[3] C. Soles, J. Douglas, W. Wu, R. Dimeo, submitted to Phys Rev E.

[4] C. Soles, J. Douglas, W. Wu, H. Peng, D. Gidley, in preparation.

[5] C. Soles, E. Lin, J. Lenhart, R. Jones, W. Wu, D. Goldfarb, M. Angelopoulos, J. Vac. Sci. Tech. B, in press.

Native and Partially Unfolded Proteins: Neutron Inelastic Scattering and Simulations

Proteins are long chain-like molecules that are intricately folded. As they function they unfold in specific ways. How proteins can quickly refold without tangling remains a central mystery in molecular biology. Partially folded proteins provide an approach to this problem, and are also important in cell functioning. The approach is that stable partially folded states have been shown to resemble the kinetic folding intermediate states along the protein-folding pathway. A molten globule (MG) is a compact partially folded protein, with a backbone resembling the completely folded protein, but lacking the extensive specific side-chain packing interactions of the native-like (i.e., properly folded) structure. A full understanding of the mechanism of protein folding requires the knowledge of the structures, relative energetics, and dynamics of the species populating the folding pathway. Incoherent inelastic neutron scattering (INS), which makes use of the large incoherent cross section of hydrogen nuclei, is a technique well suited to the study of protein internal molecular motion on the picosecond time scale. Molecular dynamics (MD) simulations, on the other hand, are a potentially valuable tool for interpreting neutron data on proteins [1, 2], and may provide atomic level description of the motions taking place.

In this study, we have explored the dynamics of bovine α-lactalbumin, a calcium-binding protein, in the native and molten globule states, using both techniques. INS data were collected on the Disk-Chopper Spectrometer at ≈ 32 μeV resolution for native and molten globular bovine α-lactalbumin. The simulations results were generated from ≈ 1 ns constant temperature and pressure MD trajectories. The model systems consisted each of a single protein monomer, immersed in a large water box (60 Å × 50 Å × 80 Å). For the native state, the α-lactalbumin configuration was initiated from the crystal structure. The model molten globule state was generated by partially unfolding the protein at 500 K at atmospheric pressure until the radius of gyration reached the experimental value determined for the molten globule state (10 % expansion). A 1 ns trajectory was then generated at 300 K for data analysis and comparison with experiment.

Figure 1 shows the structure of the α-lactalbumin in the native and molten globule states obtained from the MD simulations in solution at 300 K. The overall structural change, manifested by the conservation of the helical α-domain and the loss of the β sheets in the β-domain, is consistent with NMR data [3]. We therefore regard this structure as a reasonable model of a member of the MG ensemble for comparison with the INS data.

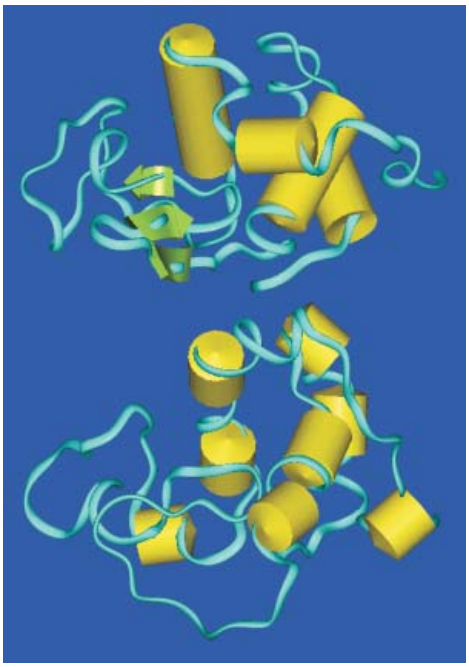

FIGURE 1. α-lactalbumin structure in the native (top) and molten globule (bottom) state from MD simulations. Note the loss of the β-domain structure, with most the α domain (helix) being conserved.

In Fig. 2 we report the incoherent structure factors $S(Q,\omega)$ as a functions of energy transfer $\hbar\omega$ for selected momentum transfer Q, measured and calculated from the MD simulations trajectories. In both systems the agreement with experiment is remarkable, assessing the ability of the simulations to reproduce the picosecond dynamics of the protein. In agreement with previous INS data collected at lower resolution [4], the molten globule has a broader quasi-elastic spectra compared to the native state, which indicates that the protein atoms are more mobile in the MG state. The additional motion is large enough to be detected at the length scale probed by the DCS spectrometer, i.e., in the range 3 Å to 60 Å.

To investigate the relationship between the structure of the protein and the motion of its side chains, we have used the MD trajectories to follow the motion of these side chains

M. Tarek
NIST Center for Neutron Research
National Institute of Standards and Technology
Gaithersburg, MD 20899-8562
and
Center for Molecular Modeling and
Department of Chemistry, University of Pennsylvania
Philadelphia, PA 19103

D. J. Tobias
Department of Chemistry
University of California
Irvine, CA 92697-632

Z. Bu and D. A. Neumann
NIST Center for Neutron Research
National Institute of Standards and Technology
Gaithersburg, MD 20899-8562

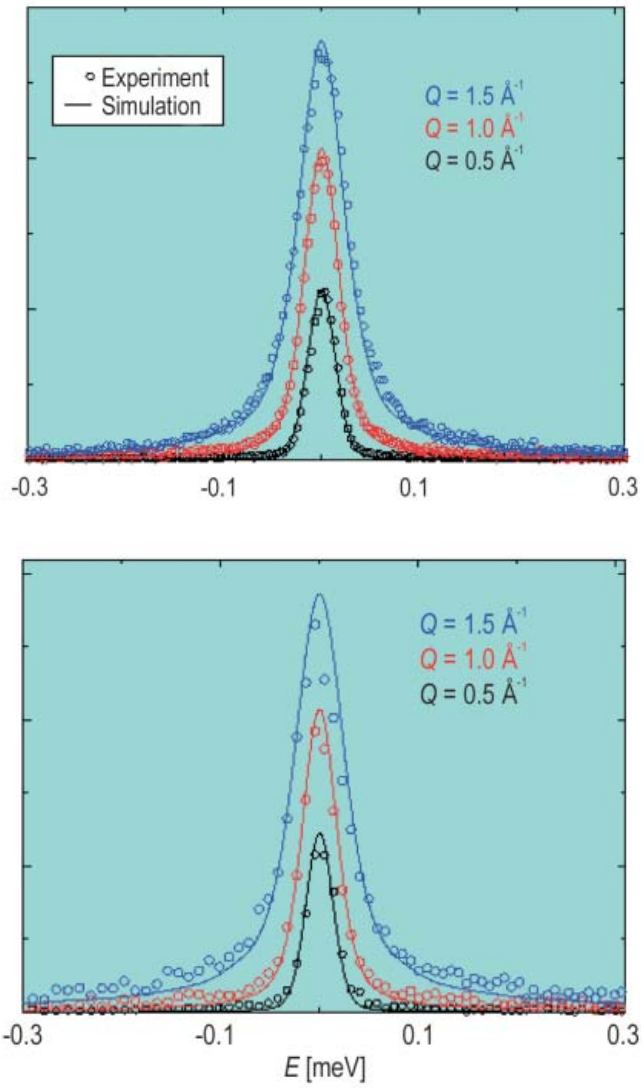

FIGURE 2. Incoherent structure factor *S(Q,ω)* at selected wavevectors *Q*, measured and calculated from the simulation for the native (top) and molten globule (bottom) states.

quantitatively. Figure 3 reports the fluctuations per residue along the backbone for the native and the molten globule states, as a function of residue. These correspond to the 100 ps root-mean-square amplitudes of motion of the backbone atoms, averaged over the simulation trajectories. First for the native state, the backbone fluctuations appear to correlate with the secondary structure of the protein, showing much smaller amplitudes in the α-helix and β-sheet regions. For the molten globule state, a significant increase in the protein fluctuation amplitudes is observed, in agreement with the broadening of the INS spectra.

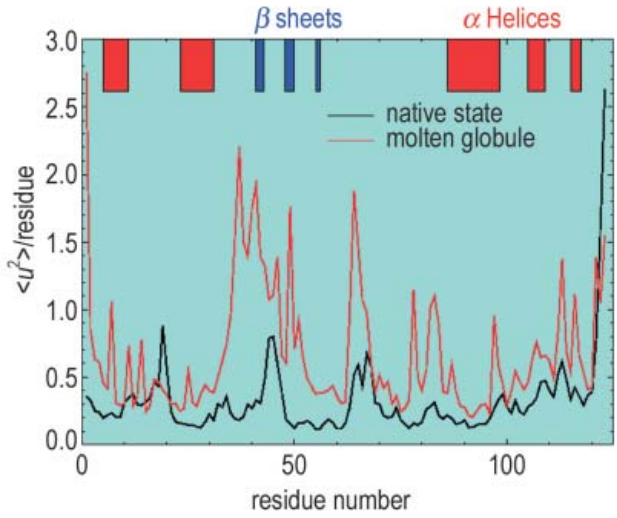

FIGURE 3. 100 ps mean squared fluctuations of the backbone atoms computed from the MD simulations of the native state (black) and the molten globule state (red).

Figure 3 shows clearly that most of the additional motion occurs in the region of the protein that "unfolds," i.e., the β-domain. The results indicate also that the motion of the side chains is by no means homogeneous. Differences in amplitudes up to 10 folds are observed between parts of the proteins, regardless of exposure to the solvent.

The MD study of the dynamics of partially folded states of the protein should in principle be extended to explore a large portion of the conformational space, i.e., be extended to a large ensemble of non-native conformers. At any rate, the present results, though limited, combined with neutron experiments are believed to capture the essence of the structural and dynamical changes taking place as the protein partially unfolds. They demonstrate the utility of the MD simulations for qualitatively elucidating the dynamical behavior of native and non-native proteins at the atomic level.

References

[1] M. Tarek, G. J. Matryna, and D. J. Tobias, J. Amer. Chem. Soc. **122**, 10450 (2000).

[2] M. Tarek and D. J. Tobias, Biophys. J. **79**, 3244 (2000).

[3] J. Baum *et al*., Biochemistry, **28**, 7 (1989).

[4] Z. Bu *et al*., J. Mol. Biol. **301**, 525 (2000).

Performance Enhancements to the CHRNS 30-m SANS Instrument

J. Cook, I.G. Schröder, S.-M. Choi*, S.R. Kline, B. Hammouda, C.J. Glinka

NIST Center for Neutron Research

* present address: Korea Advanced Institute of Science and Technology

Two changes made to the optics of the CHRNS 30-m SANS instrument during the installation of the NCNR's new cold source have increased the flux at the sample *and* the low-Q resolution of the instrument.

The increase in flux, over and above that provided by the new cold source, comes from replacing the instrument's cooled bismuth-beryllium filter with an "optical filter" of the type shown schematically in Figure 1. The optical filter replaces 10 meters of straight neutron guide, and its 40-cm long Bi-Be filter, with an inclined guide section with a high critical angle supermirror reflective coating. The optical filter channels cold neutrons, with wavelengths as short as 3 Å, out of the line-of-sight of fast neutrons and gamma rays from the source. The cold neutrons delivered to the SANS instrument undergo an even number of reflections in the optical filter to emerge in the horizontal direction, but displaced 15 cm vertically. To accommodate the beam displacement, the entire SANS instrument had to be raised; a non-trivial task that required detailed engineering analysis, careful planning and skilled execution.

The design of the optical filter was refined with the aid of detailed Monte Carlo calculations of the angular and spectral distribution of neutrons transmitted by the optical filter. Figure 2 shows the calculated and measured gain in flux at the sample, due to the optical filter alone, for the supermirror reflectivity model shown in the inset. These

results demonstrate that the optical filter transmission is about the same as the previous crystal filter for wavelengths around 5 Å, but becomes substantially better at longer wavelengths where absorption in the crystal filter becomes significant.

The optics for the CHRNS SANS instrument were further improved by installing a system of refracting lenses and prisms near the sample position to focus 17 Å neutrons onto the detector at its maximum distance, 13 m, from the sample. A similar lens system, consisting of 28 biconcave single crystals of MgF_2 for focusing 8 Å neutrons, has been in use on the NCNR's other 30-m SANS instrument on guide NG-7 for nearly two years [1]. The refracting power of the lenses increases with the wavelength squared, but so does the distance the neutron falls between the sample and detector due to gravity. The vertical spreading of the focus for a beam with a wavelength spread typical of a SANS instrument, about 10-15% FWHM, restricts the utility of the lenses alone to wavelengths less than 10 Å. The new development implemented on the CHRNS SANS instrument was to follow the lenses with prisms that refract in the vertical direction to counteract the effect of gravity.

Figure 3 depicts the arrangement of lenses and prisms now installed on the CHRNS SANS instrument. Seven MgF_2 biconcave lenses focus 17 Å neutrons at the detector, 13 m from the sample. For this distance a single prism with an apex angle of 161º would cancel the beam spreading due to gravity *for all wavelengths* [2]. Such a prism, however, would have to be 250 mm long at its base to intercept the full beam height transmitted by the lenses (~ 2 cm). A more practical scheme, as shown in Figure 4, is to stack two sets of prisms, with each prism 30 mm long and 5 mm high with an apex angle of 143º, to

give the same anti-gravity effect. In this scheme, the bottoms of each prism are coated with Gd_2O_3 to eliminate surface reflections.

The effectiveness of the lens/prism combination can be seen in Figure 4 which compares circularly averaged SANS data from voids in an irradiated crystal of aluminum obtained with pinhole collimation and with the focusing optics. The data for the lens/prism system extend to a minimum scattering vector Q = 0.00045 $Å^{-1}$, nearly a factor of two lower than the pinhole collimation. Furthermore, the scattered intensity is 3 times higher with the lens/prism system because a larger area of the sample can be illuminated without degrading the Q-resolution. With pinhole collimation, intensity at the detector is roughly proportional to Q^4_{min}, hence the lens/prism system represents an overall intensity gain of 48 compared with simply reducing pinhole aperture size to achieve the same minimum Q. The new cold source and improvements in optics are enabling microstructural studies that link nanoscale with microscale features in, for example, polymer-clay nanocomposites, gels, and fluxoid lattices in superconductors.

REFERENCES

[1] S.-M. Choi, J.G. Barker, C.J. Glinka, Y.T. Cheng, P.L. Gammel, *J. Appl. Cryst.* **33**, 793 (2000).

[2] E.M. Forgan, R. Cubitt, *Neutron News* **9(4)**, 25 (1998).

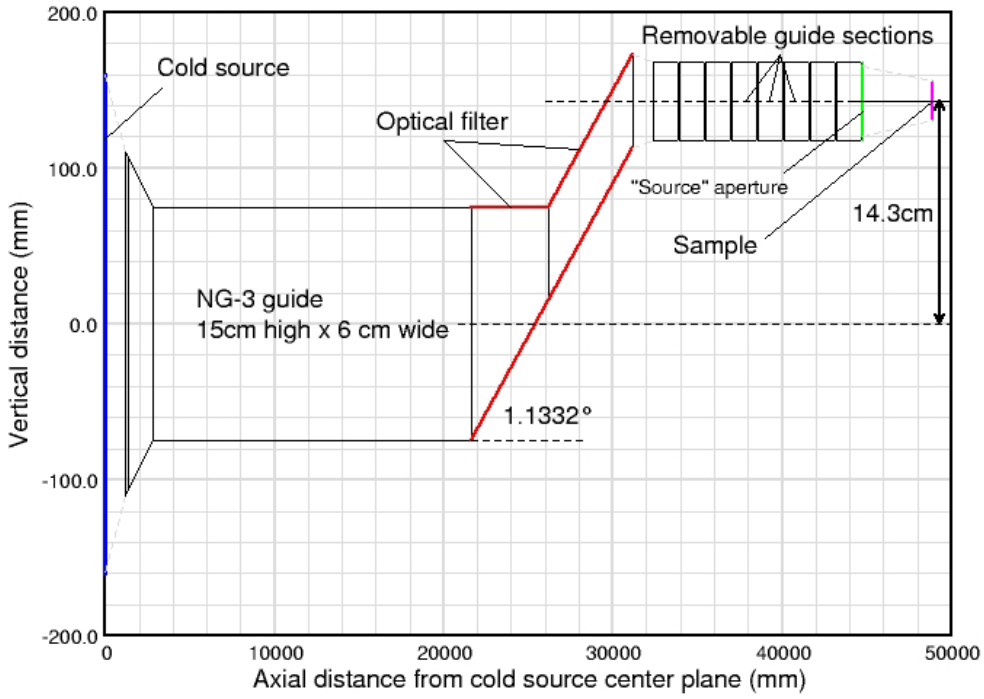

Figure 1. Schematic elevation of the NG-3 optical filter (note vertical scale is exaggerated for clarity). The inclined section shown in red is coated with supermirror with critical angle ≈ 3.2 times that of natural nickel. The removable guide sections are in the pre-sample flight path of the CHRNS SANS instrument.

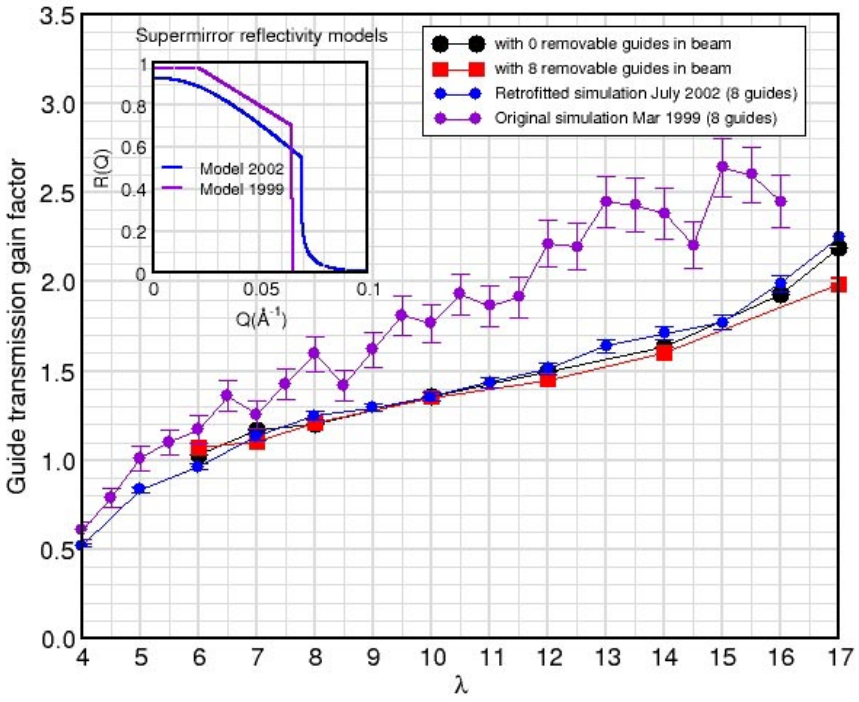

Figure 2. Transmission gains of the NG-3 optical filter. The black circles are measured with no removable guides in the beam. The red squares are measured with 8 removable guides in the beam. The violet circles are the original Monte Carlo simulated gain predictions (March 1999) using the supermirror reflectivity model shown in the inset. The blue circles are simulated gains (July 2002) using the refined reflectivity model shown in the inset. These "hindsight" simulations predict the measured gains well for M=3.2 supermirror with R(Q=0)=0.930 and RMS surface roughness=10Å with R(Q=0.069Å^{-1})=0.55.

- Correction of Gravity Effect with Prisms

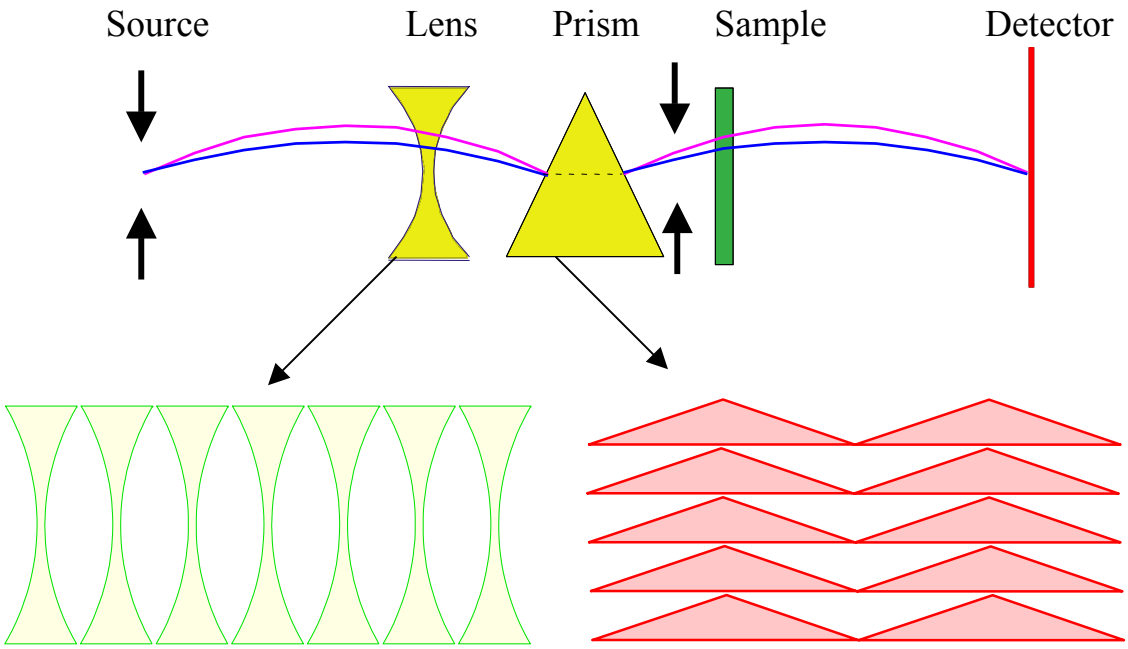

Figure 3. Schematic diagram of the configuration of lenses and prisms used on the 30-m CHRNS SANS instrument. The seven biconcave lenses focus 17 Å neutrons at the detector, 13 m from the sample, and the double stack of prisms refracts the beam vertically to cancel the effect of gravity.

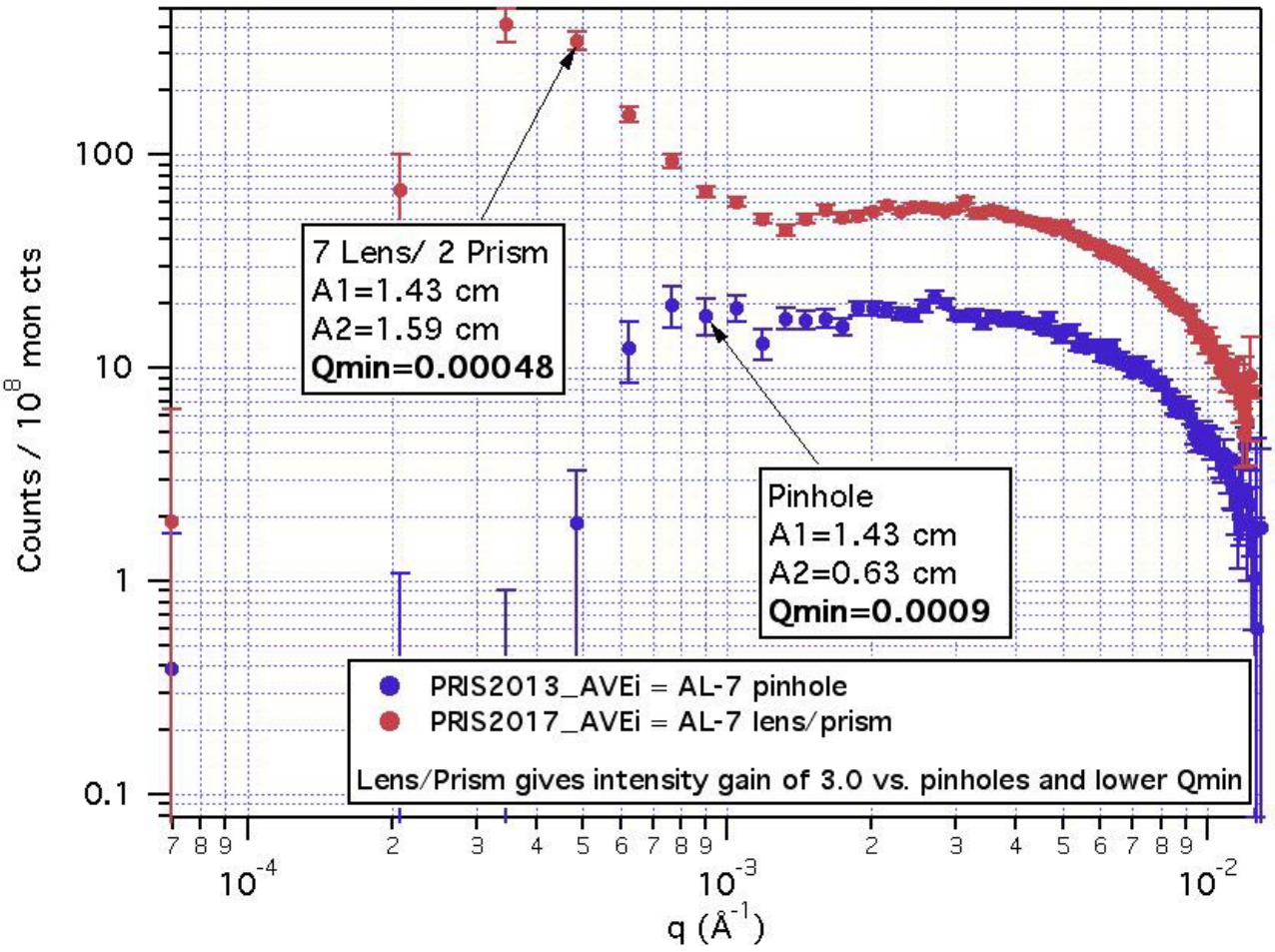

Figure 4. SANS from voids in an aluminum crystal measured with and without the new focusing and gravity cancellation optics installed on the CHRNS SANS instrument. The optics halve the minimum accessible Q-value while increasing the scattered intensity roughly threefold.

EMERGENT EXCITATIONS IN A GEOMETRICALLY FRUSTATED MAGNET

Systems where a large diversity of states are involved are common in biology, chemistry and physics.[1,2] Notable examples are glasses, liquids and proteins. An essential concept in understanding those systems is frustration, i.e., the degrees of freedom cannot be optimized simultaneously due to competing interactions. Magnetic systems offer extreme examples in the form of spin lattice, where all interactions between spins cannot be simultaneously satisfied. Such geometrical frustration can lead to macroscopic degeneracies and qualitatively new states of matter.

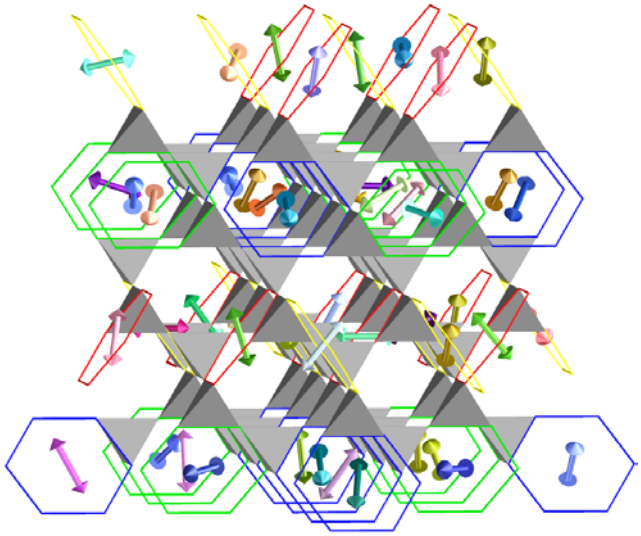

Fig. 1 The lattice of corner-sharing tetrahedra formed by the octahedrally coordinated B sites in a spinel structure with chemical formula AB_2O_4. A periodic assignment of all spins in the pyrochlore lattice is made to four different types of non-overlapping hexagons, represented by the colors blue, green, red, and gold. Every spin belongs to just one hexagon and each such hexagon carries a six spin director. The resulting tetragonal structure of these hexagons has a unit cell of $2a \times 2a \times 3c$ and can be described by a stacking of two different types of three-layer slabs along the c-axis. The hexagon coverage on consecutive slabs is in fact uncorrelated, so that a macroscopic number of random slab-sequences can be generated.

To explore this possibility, we examined magnetic fluctuations in $ZnCr_2O_4$.[3] The B-site of this spinel lattice occupied by spin-3/2 Cr^{3+} leads to a magnet with dominant nearest neighbor interactions on the lattice of corner-sharing tetrahedra[4] shown in Fig. 1. Because the spin interaction energy is minimized when the four spins on each tetrahedron add to zero, interactions do not call for a long-range order, but simply define a restricted phase space for fluctuations. Just as composite fermions can emerge from degenerate Landau levels in a two-dimensional electron gas, the near degenerate manifold of states in a frustrated magnet is fertile ground for emergent behavior[5].

Neutron scattering provides the most effective tool to study possible composite spin degrees of freedom by directly probing the form factor of such entities. Fig. 2 (a) and (b) show the wave vector dependence of the low energy inelastic neutron scattering cross section in the spin liquid phase of $ZnCr_2O_4$. The data exhibit broad maxima at the Brillouin zone boundaries, signaling the emergence of confined nano-scale spin clusters. Rather than Fourier-inverting the data, we consider potential spin clusters and test the corresponding prediction for the form factor against the data. Individual tetrahedra would be prime candidates as they constitute the basic motif of the pyrochlore lattice. However, a tetrahedron is too small to account for the observed features. The next smallest symmetric structural unit is the hexagonal loop formed by a cluster of six tetrahedra [Fig. 3]. Two spins from each tetrahedron occupy the vertices of a hexagon while the other two spins from each tetrahedron belong to different hexagons. It is possible to assign all spins on the spinel lattice to hexagons simultaneously thus producing N/6 weakly interacting degrees of freedom [Fig. 1]. An outstanding fit is achieved for the antiferromagnetic hexagonal spin loops as evidenced by Fig. 2 (c) and (d). Thus rather than scattering from individual spins, neutrons scatter from antiferromagnetic hexagonal spin clusters. In effect, $ZnCr_2O_4$ at low temperatures is not a system of strongly interacting spins, but a protectorate of weakly interacting spin-loop directors. Since the six hexagon spins are anti-parallel with each other, the staggered magnetization vector for a single hexagon, which shall be called the spin loop director, is decoupled from the 12 outer spins, and hence its

S.-H. Lee, Q. Huang
NIST Center for Neutron Research
National Institute of Standards and Technology
Gaithersburg, MD 20899-8562

C. Broholm, G. Gasparovic
Department of Physics and Astronomy
The Johns Hopkins University
Baltimore, MD 21218

T.H. Kim
Francis Bitter Magnet Laboratory
Massachusetts Institute of Technology
Cambridge, MA 02139

W. Ratcliff, S-W. Cheong
Department of Physics and Astronomy
Rutgers University
Piscataway, NJ 08854

reorientation embodies the long-sought local zero energy mode for the pyrochlore lattice.

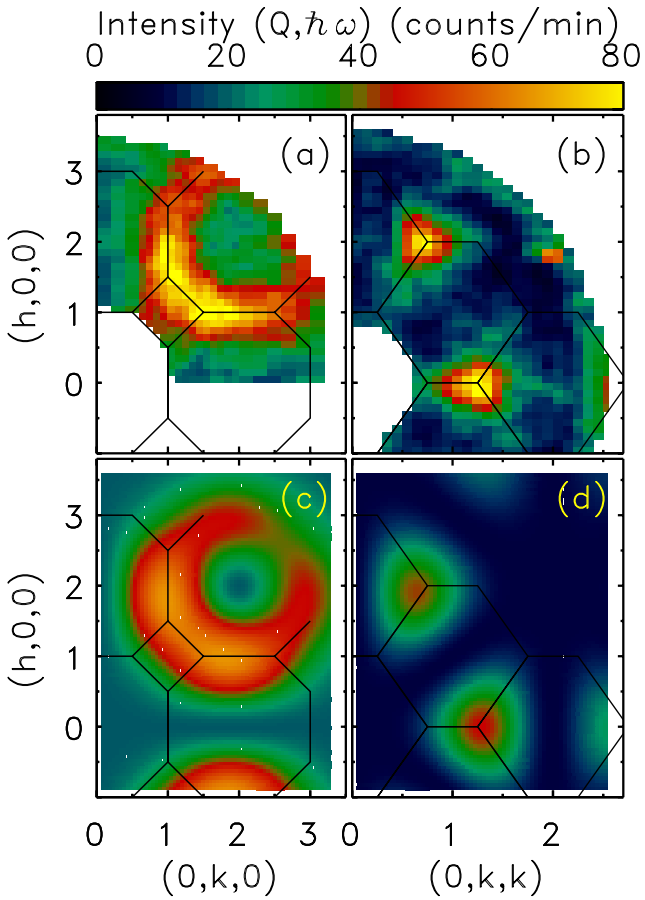

Fig. 2 (a)-(b) Color images of inelastic neutron scattering intensities from single crystals of $ZnCr_2O_4$ in the (hk0) and (hkk) symmetry planes obtained at T=15K for $\hbar\omega$ = 1 meV. The data are a measure of the dynamic form factor for self-organized nano-scale spin clusters in the material. (c)-(d) Color images of the form factor squared calculated for antiferromagnetic hexagon spin loops averaged over the four hexagon orientations in the spinel lattice. The excellent agreement between model and data identifies the spin clusters as hexagonal spin loops.

Composite degrees of freedom are common in strongly interacting many body systems. Quarks form hadrons, hadrons form nuclei, nuclei plus electrons form atoms, atoms form molecules, which in turn are the basis for complex biological functionality. Planets, stars, galaxies and galaxy clusters are examples of clustering on a grander length scale. However, to our knowledge, the emergence of a confined spin cluster degree of freedom has not previously been documented in a uniform gapless magnet. The discovery is important because magnets offer an opportunity not afforded by the aforementioned systems to monitor emergent structure in complex interacting systems with microscopic probes such as neutron scattering and NMR. The collapse of a geometrically frustrated magnet into a director protectorate could for example be a useful template for exploring aspects of protein folding[2].

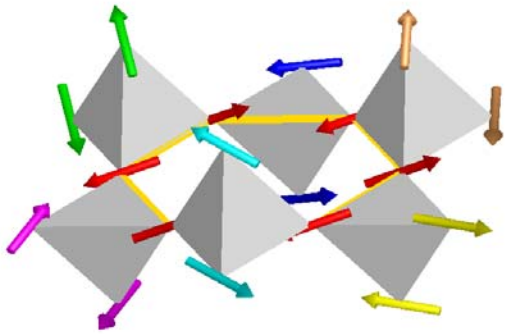

Fig. 3 : Spin cluster surrounding a hexagon (shown in gold) in the pyrochlore lattice of Fig. 1.

REFERENCES

[1] P. G. Debenedetti et al., *Nature* **410**, 259 (2001).

[2] P. G. Wolynes and W. A. Eaton, *Physics World* **12**, 39 (1999).

[3] S.-H. Lee, C. Broholm, W. Ratcliff, G. Gasparovic, Q. Huang, T.H. Kim, and S-W. Cheong, *Nature*, in press (2002).

[4] S.-H. Lee et al., *Phys. Rev. Lett.* **84**, 3718 (2000).

[5] R. B. Laughlin and D. Pines, *Proc. Natl. Acad. Sci. U.S.A.* **97**, 28 (2000).

SUMMER SCHOOL ON SANS AND REFLECTOMETRY HELD AT NIST*

The National Institute of Standards and Technology's (NIST) Center for Neutron Research (NCNR) held its eighth annual Summer School on Neutron Scattering at the reactor on the NIST campus in Gaithersburg, Maryland, on June 3-7, 2002. The course this year focused, as it does every two years, on the complementary techniques of small-angle neutron scattering (SANS) and neutron reflectometry (NR). An enthusiastic group of 40 graduate students and postdocs, predominantly from university chemical engineering and materials science departments, attended (see photo); the largest class so far. Some of the participants had attended the NCNR's course on cold neutron spectroscopy that was given last year and alternates with the SANS/NR course.

This year's course differed in two respects from previous years. First of all, the NCNR's perfect-crystal diffractometer for ultra-high resolution SANS was an integral part of the course for the first time. The availability of this instrument, in addition to the NCNR's two 30-m pinhole collimation SANS instruments and two reflectometers, made it possible to increase the class size to 40 students while maintaining groups of no more than 8 students working closely with staff in the hands-on portions of the course. The other major difference was an increased emphasis on having the students carry out complete experiments on the instruments, including reducing and analyzing the data. The intent here was to introduce much of the practical material that had been covered in lectures in past courses in the context of performing a specific experiment. Hence the experiments were preceded and punctuated with less formal presentations in small conference rooms that focused on engaging the students in interactive discussions of all aspects of the experiments, from assessing feasibility, optimizing sample geometry and instrument configuration, planning counting times, sample environments, and methods of data reduction and analysis. The small group sessions were preceded by only three formal lectures that introduced the fundamentals of SANS and reflectometry and some of the main application areas for the techniques.

For the SANS experiments, samples were chosen with structure that gave scattering in both the SANS and USANS regimes. Thus, for example, some of the students made both SANS and USANS measurements on a semi-dilute solution of sodium Montmorillonite clay dispersed in D_2O. The dispersed clay platelets have large aspect ratios (diameter/thickness ~ 1000). Fully characterizing the structure thus requires measurements over a wide Q-range. The student groups who worked at the 30-m SANS instrument on guide NG3 measured the temperature dependence of the composition fluctuations that precede phase separation in a polyolefin blend. From these data, the spinodal temperature and interaction parameter, χ, were obtained. A sample of the same blend that had been allowed to phase separate was examined on the USANS instrument in order to estimate the size of the phase-separated domains.

The NCNR's horizontal sample geometry reflectometer was used to investigate Langmuir monolayers of diblock copolymers at the air-liquid interface. Three groups of students did the same experiment over the course of the week, each using a different molecular weight polymer. Each group also analyzed its data in three different ways to get a feel

for the strengths and weaknesses of each method. The three groups combined and compared their results with theories of the molecular weight dependence of the chain segment density versus depth below the surface. The groups who worked at the NCNR's vertical sample geometry reflectometer were given a puzzle to solve. With only minimal information about the multilayer structure of a coating on a silicon substrate, the groups were challenged to develop a consistent model of the scattering length density (SLD) depth profile by fitting to the reflectivity data. Additional measurements made for the same coating, but with a different reference substrate, were then used to demonstrate a model-independent phase-sensitive technique for inverting the data to directly obtain the true SLD profile of the multilayer, an alkanethiol monolayer attached to a gold sublayer on top of a chromium layer, deposited on either silicon or sapphire as the substrate.

The experiments were completed by midday on Thursday; partly to allow the student groups time to prepare short talks about their results for Friday afternoon's final session. The course returned to a lecture format on Friday morning with talks on current SANS research in polymers, and colloids and microemulsions given in parallel with talks on recent reflectivity work done at the NCNR on polymers at surfaces and interfaces, and on three examples of technologically important magnetic multilayer materials.

Based on the evaluation forms they filled out, the students found the course to be very worthwhile and were most appreciative of the time and attention they received from the 16 scientific staff members involved. The students had the added benefit of hearing and interacting with two invited speakers, Robert Briber, University of Maryland, who lectured on SANS from Polymers on Friday morning, and Michael Kent, Sandia National Laboratory, who teamed with Sushil Satija in leading the groups who did the reflectivity experiments on diblock copolymers at a liquid surface.

The summer school this year was once again made possible through support provided by the NCNR, with matching support from the National Science Foundation's Center for High Resolution Neutron Scattering (CHRNS) at NIST, in the form of assistance with travel expenses for the university students.

Charles Glinka
NIST Center for Neutron Research
Gaithersburg, MD, USA

*preprint of a meeting report to appear in *NEUTRON NEWS* (in press, 2002).

Students and staff who participated in the eighth annual NCNR/CHRNS Summer School on Neutron Scattering at the NCNR, June 5-9, 2002. One-quarter of the participants were either women or minorities.